AN ANALYSIS OF THE STRIATED MUSCLE FIBER ACTION CURRENT

HOWARD JENERICK
From the Department of Physiology, Emory University, Atlanta

ABSTRACT A method is presented for determining the magnitude of the ionic current associated with the propagated spike potential. Parameters of the action current are then compared to various aspects of the response as recorded in a phase plane. The findings also include evidence for (*a*) Na^+ ion as the major inward current carrier, (*b*) a fairly constant membrane conductance during the terminal phase ($\sim$1 msec.) of the spike potential, and (*c*) the influence of Ca^{++} ion concentration on the action current.

INTRODUCTION

Measurements of the current-voltage relationship in isolated giant axons by means of the voltage-clamp technique (Cole, 1949; Hodgkin and Huxley, 1952) have led to the postulate of several time- and voltage-dependent membrane conductances. These work in conjunction with the ionic concentration gradients for sodium and potassium ions, to generate the action current. For a variety of reasons, the striated muscle fiber has not yet yielded to this particular method and comparable, experimental data on the genesis of the action current by this cell are not available. However, it seems likely that similar events occur in muscle fibers, and that the ionic currents associated with the propagated impulse bear a relation to the driving forces inherent in the transmembrane ionic concentration gradients. The present study of the muscle spike potential is an attempt to obtain this information and to examine the relationship between the membrane voltage and the membrane ionic current as these are reflected in the phase plane trajectory of the response.

METHODS

Experimental Methods. Propagating action potentials from single, surface fibers of the isolated sartorius muscle of *Rana pipiens* were obtained by means of intracellular glass microelectrodes (tip potentials < 4 mv; resistance, 2 to 8 megohms) and a neutralized input capacitance DC preamplifier (Argonaut LRA 043). All responses were recorded simultaneously in the phase plane (V, dV/dt) and in a conventional coordinate system (V, t), (see Jenerick, 1963*a*, for details). Since significant frequency components above a few kilocycles were not identified in the muscle action potential, the

upper frequency limit of the recording apparatus was customarily set at 10 kc (3 db down) to limit noise. Incidentally, no differences in recorded spikes were noted whether the cut-off was lowered to 8 kc or raised to 16 kc.

It was observed that the response of the microelectrode and neutralized input capacitance preamplifier could not be properly compensated by observation of the rise time to an applied step voltage. (The resistance and the shunt capacitance of the electrode are distributed properties, and do not constitute a single stage, low pass filter for which such amplifiers are designed.) To obviate this possible source of error, the microelectrode frequency response was always adjusted by means of a series of sine wave calibrating frequencies with primary attention being given to a uniform gain-frequency response over the selected pass band of 10 kc.

The standard Ringer's fluid contained 110 mM NaCl, 2.5 mM KCl, 2.0 mM $CaCl_2$, and was buffered to pH 7.2 — 7.4 with 1.5 mM phosphate. Room temperatures varied between 22° and 25°C. In experiments in which sodium chloride concentrations were lowered, sucrose or choline chloride was used to maintain isotonicity.

Analytical Methods. It is first assumed that the membrane action current of any surface-lying muscle fiber conducting a propagated impulse obeys the cable equation (Hodgkin and Huxley, 1952). This equation related the total transmembrane current density to the sum of a capacitative current and an ionic current,

$$\frac{a}{2R\Theta^2}\frac{d^2V}{dt^2} = C\frac{dV}{dt} + I \tag{1.1}$$

where a is the fiber radius, R is the myoplasm resistivity, Θ is conduction velocity, V is transmembrane voltage, t is time, C is membrane capacitance, and I is the *ionic* current density. Note that the equation as written, includes the simplifying assumption that $r_i + r_o \simeq r_i$, where r_i is the resistance of the myoplasm per unit length and r_o is the resistance of the bathing fluid per unit length. Although it might appear that this condition cannot be met strictly without resort to isolated single fibers, we have on occasion deliberately recorded spike potentials from subsurface fibers. These responses resemble those obtained from surface fibers as used in this study closely enough to suggest that the resistance of the external fluid surrounding the muscle fiber is negligible as assumed.

The foot of the spike potential rises exponentially in time and is transformed into a linear trajectory of slope k in the phase plane (Fig. 1*a* and *b*). Since $k = 2RC\Theta^2/a$, (Jenerick, 1957), Equation (1.1) may be recast,

$$\frac{d^2V}{dt^2} = k\left(\frac{dV}{dt} + \frac{I}{C}\right)$$

Following a procedure suggested by Minorsky (1947), let $x = dV/dt$, then $dx/dt = d^2V/dt^2$. By substitution and subsequent use of the chain rule, it follows that,

$$\frac{dx}{dt} = k\left(x + \frac{I}{C}\right)$$

$$\frac{dV}{x} = \frac{dx}{k(x + I/C)}$$

$$\frac{dx}{dV} = \frac{k(x + I/C)}{x} \tag{1.2}$$

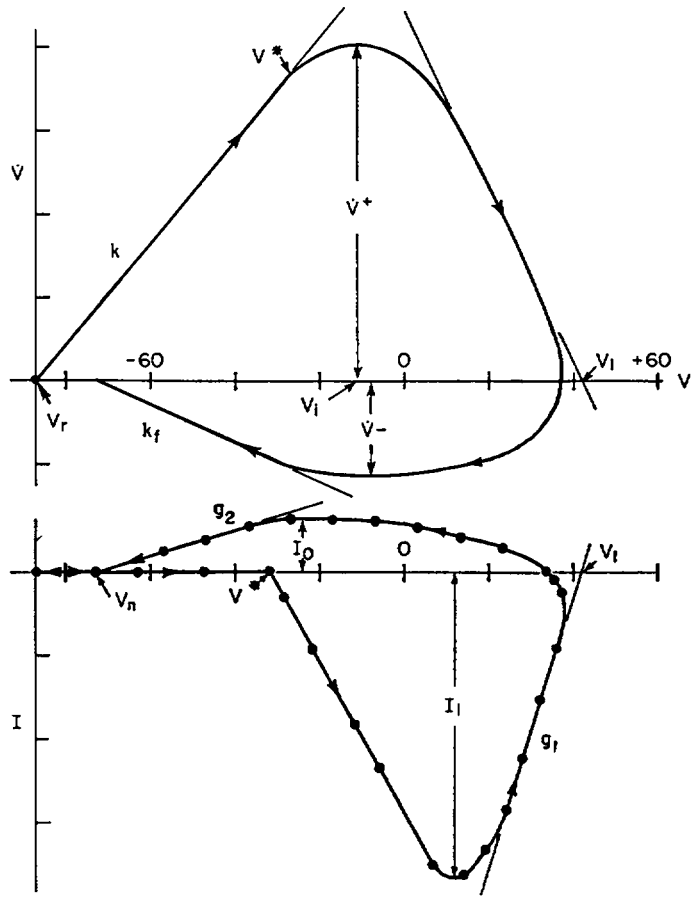

FIGURE 1*a* A tracing of a spike potential recorded as a phase plane trajectory (above) and the calculated action current (below). The resting potential of −88 mv is indicated at the left of both responses which develop in time as shown by the arrows. The dots represent calculated coordinate points for the action current through which a smoothed line was drawn. $\dot{V}$ scale units are 100 V/sec., I units are 1 ma/cm², and V units are 20 mv, while the symbols are defined in the text.

From the original definition of x, it is also seen that

$$\frac{dx}{dV} = \frac{d(dV/dt)}{dV} \tag{1.3}$$

The coordinates of the phase plane are $(V, dV/dt)$, hence, the *slope* of the spike trajectory at any point is equal to the right-hand member of (1.3). Defining this slope as m, and reintroducing dV/dt for x in (1.2),

$$m = \frac{k(dV/dt + I/C)}{dV/dt}$$

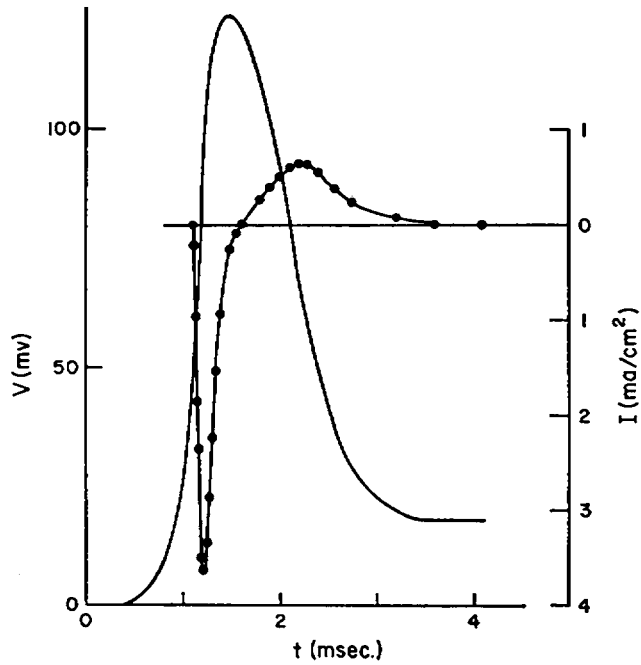

FIGURE 1*b* The action current of Fig. 1*a* plotted against the recorded spike potential in conventional coordinates. Note the current reversal following the attainment of the peak spike potential, and the marked decline in outward current as the spike response approaches the negative after-potential.

Solving for I/C and writing dV/dt as $\dot{V}$, we finally obtain

$$I/C = \dot{V}\left(\frac{m}{k} - 1\right). \tag{1.4}$$

Thus, by appropriate substitution, (1.4) permits a point by point evaluation of I/C, the (ionic current/membrane capacitance) ratio from any phase trajectory.

In the present work all I/C ratios were converted to currents, I, (in ma/cm²) by multiplication by a value of 5 μf/cm² for C (taken from Hubbard, 1963).

While it is a direct graphical procedure to determine $\dot{V}$ and k from tracings of the phase plane trajectory, the following variety of methods were employed in the present study to obtain the slope m of the trajectory. The most straightforward determination of m was by means of a calibrated slope indicator (such as the Gerber derivimeter). It was also possible to measure m with a protractor and a cylindrical lens (a stirring rod) to amplify the tracing in any selected region of the response. The slope was occasionally obtained analytically from several exact equations fitted to successive portions of the phase plane record (Jenerick, 1961). Alternatively, it was assumed that any sufficiently small segment of the trajectory would be approximated by a portion of a parabola. This latter procedure exploits a well known property of parabolas which is that the slope $m = dy/dx$ at the point x, y is equal to $\Delta y/\Delta x$ where $\Delta y = y_{+\Delta} - y_{-\Delta}$ and $\Delta x = x_{+\Delta} - x_{-\Delta}$. Numerical

calculations were made from a list of coordinate points taken at equal intervals, h, (5 or 10 mv) on the V axis of the trajectory. Although this approximation deteriorates in regions near the peak of the spike, as compared to direct measurements of slope, it provides a rapid survey of the general character of the action current response.

DEFINITIONS

V	Transmembrane voltage (mv)
V_r	Resting membrane potential (mv)
V_s	Maximum spike potential (from V_r) (mv)
V_1, (V_{Na})	Equilibrium potential for inward current (mv)
V^*	Excitation potential (from V_r) (mv)
V_i	Potential at 1st inflection point (mv)
$\dot{V}$	First time derivative of spike (V/sec.)
$\dot{V}+$	Maximum rate of rise of spike (V/sec.)
$\dot{V}-$	Maximum rate of fall of spike (V/sec.)
k	Rate constant for spike foot (msec.$^{-1}$)
k_f	Rate constant for terminal portion of spike (msec.$^{-1}$)
g_1, (g_{Na})	Limiting membrane conductance for inward current (mmhos/cm^2)
g_2	Limiting membrane conductance for outward current (mmhos/cm^2)
I	Transmembrane ionic current (ma/cm^2)
I_i	Peak inward ionic current (ma/cm^2)
I_o	Peak outward ionic current (ma/cm^2)

RESULTS AND DISCUSSION

Current-Voltage Relationship. By means of the methods outlined above, the ionic current was calculated from enlarged tracings of the propagating action potential recorded in the phase plane. The reconstructed action current of a typical response is plotted in Fig. 1 against voltage (a) and against time (b). Tracings of the original records are also shown and prominent features of the response are labeled. Prior to the attainment of V^*, depolarizing current is drawn predominantly from the membrane capacitance as the action potential invades the recording site. Such capacitative current is irrelevant to the present study and is not treated further. The *ionic* current drawn at this time through the resting membrane conductance (~0.4 mmhos/cm^2) is too small to be shown on the scale employed here. Following membrane excitation at V^*, the inward current develops rapidly in time and is usually observed to be fairly linear with voltage during the period of negative conductance (Fig. 1a). Shortly after I_i is reached, the membrane exhibits a constant conductance g_1, for a brief period, during which the inward current declines linearly toward V_1. Note that this equilibrium potential may be obtained from either plot in Fig. 1a (see also Jenerick, 1963a). Following the attainment of the peak spike height V_s, the current reverses and shortly after reaching I_o declines linearly with

voltage (membrane conductance = g_2), toward the initial value of the negative after-potential V_n. During the decay of the after-potential the ionic current is again too small to resolve by the present methods.

Since the calculated currents were obtained from the phase plane record at the expense of a considerable effort, a systematic comparison was made for predictive purposes, between the main features of the *I-V* response and various parameters of the phase plane trajectory shown in Fig. 1*a*.

Peak Inward Ionic Current, I_i. Calculations for I_i bear a close relationship to the maximum rate of rise of the spike potential, $\dot{V}+$ (Fig. 2). The data shown in the figure plot the averaged results of approximately 100 separate experiments (4 to

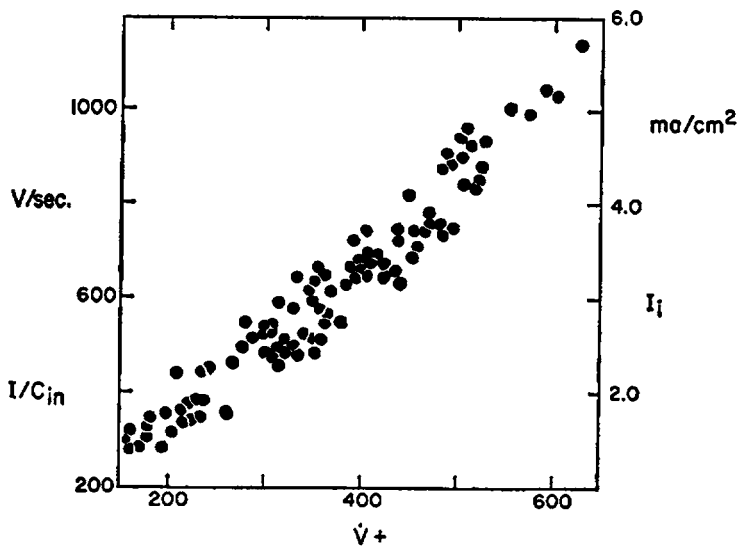

FIGURE 2 The peak inward ionic current density I_i and its equivalent, I/C_{in}, as a function of the maximum rate of rise ($\dot{V}+$) of the spike in *V*/sec. Each plotted point represents the average of a single experiment on 4 to 20 separate fibers.

20 individual responses per experiment). The conditions under which these data were obtained include (1) modified Ringer's fluid; (Na^+) 22 to 110 mM, (K^+) 0 to 8 mM, (Ca^{++}) 1 to 10 mM, pH 5.0 – 10.6, (2) Na-loading (overnight storage of isolated muscles at 4°C in 120 mM Na^+, 0 mM K^+, 2 mM Ca^{++} fluid), and (3) incipient conduction block induced by 10 mM cupferron, a trace metal chelating agent. Considering the number and variety of these experiments, it appears likely that the magnitude of $\dot{V}+$ is a reliable index of the peak inward current (as was assumed by Weidmann, 1955). This requires that the membrane capacitance remain unaltered by the various treatments, otherwise the correction explained above of the *I/C* ratio of Equation (1.4) would be invalid. As a matter of fact, the relatively

minor scatter of data in the figure seems indicative of a *constant* capacitance, since it appears somewhat unlikely that the various experimental conditions represented by the data would so similarly affect I and C that their ratio would remain linked to $\dot{V}+$. It will be tentatively assumed therefore that the capacitance was unchanged by the experimental treatments employed here, and the term "ionic current" will henceforth be used in the place of the precise term I/C.

Peak Outward Current I_o. The maximum outward current occurs shortly after the second inflection point of the spike potential as shown in Fig. 1. This inflection point is identified in the phase plane trajectory at the maximum rate of fall $\dot{V}-$. Because I_o always occurs in a region where $m \simeq 0$ in Equation (1.4), it can be expected that $(I_o/C) \simeq \dot{V}-$. Although the extensive number of calculations represented by the previous figure were not carried out for I_o, the results obtained from over 60 separate responses are shown in Fig. 3, and represent data from ex-

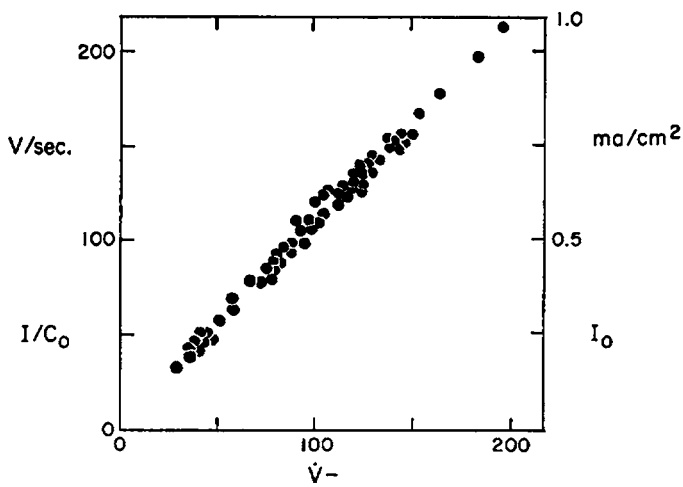

FIGURE 3 The close correlation between the peak outward ionic current density I_o (or I/C_o) and the maximum rate of fall ($\dot{V}-$) of the spike.

periments involving modified Ringer's fluid, (Na^+) 22 to 110 mM, (K^+) 1 to 5 mM, (Ca^{++}) 1 to 10 mM, and pH 5.5 − 9.2. Since the data for I/C lie well within ±10 per cent of a least squares regression line (not shown), and are independent of calculations for I_i, this is again strongly suggestive of an unaltered membrane capacitance.

Excitation Potential V^*. As shown in Fig. 1*a*, the I-V relationship of the active membrane initially passes through a region of negative conductance. The linearity of this region permitted an estimate of the membrane firing potential by a backward extrapolation to the V axis. The firing point was also identified in the original phase plane trajectory at the first deflection of the response from the initial

linear portion k. As may be inferred from inspection of the trajectory shape, V^* lies fairly close to V_i and a rough correlation is observed (Fig. 4). The conditions under which these data were obtained are similar to those outlined above (*e.g.* variable Na^+, K^+, Ca^{++}, pH). Note that V^* is considerably greater than the potential at which the local response or the activation of inward sodium current is initiated at a stimulating cathode (Jenerick, 1959). This probably arises from the fact that the change in membrane sodium conductance following "excitation" is not instantaneous. If the responsible processes are triggered by a 15 mv depolarization from the resting potential (Fig. 2 of Jenerick, 1959), but have not grown large enough to be discerned in a propagating spike by the present methods until the appearance of V^*, it is possible to make estimates of the time "lag" (*i.e.* the time lapse between the attainment of the "sodium" activation potential and of V^* in the spike). Such lag times are customarily in the order of a few hundred microseconds. Incidentally, the explosive growth in time of the inward current (Fig. 1*b*) indicates that this delay more closely resembles a true time lag than it resembles a period of slow development of the conductance change. Similar reasoning applied to the time lapse between the attainment of the "potassium" activation potential and the first appearance of the outward current (at the "break" in g_1) indicates that the outward current lag is nearly double that of the inward current, ~500 μsec.

The Inward Current Carrier. The widespread assumption that Na^+ ion

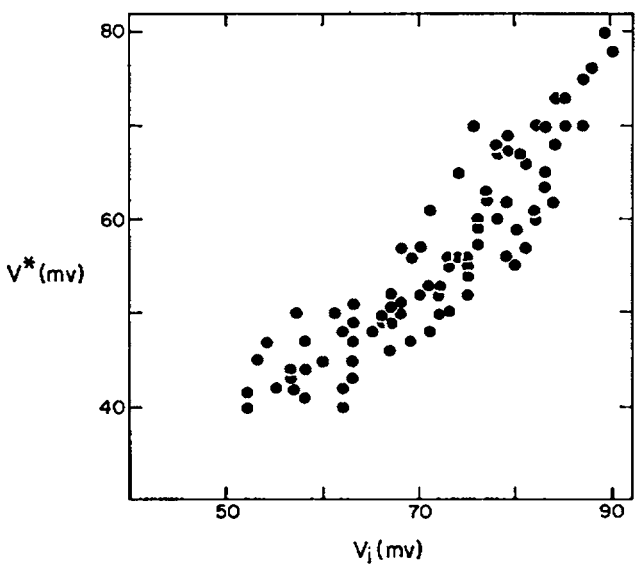

FIGURE 4 The empirical relationship between the firing potential V^* and the potential at the first inflection point of the spike, V_i. Note that V^* is 10 to 15 mv smaller than V_i. This indicates that membrane excitation occurs *prior* to the appearance of the first inflection point.

carries the inward current of the muscle spike potential was tested by seeking experimental verification of the following requirements implicit in the assumption: (*a*) the equilibrium potential V_1 of the inward current should vary *logarithmically* with external Na^+ concentration, with slope = 59 mv/decade, (*b*) the maximum membrane conductance g_1 should be *independent* of (Na^+), and (*c*) the peak current I_t should vary *linearly* with (Na^+). The latter is probably a less strict requirement for propagating spike potentials in which time and propagation velocity play an important role; however, *all* requirements were met. Fig. 5 shows typical unselected responses from one muscle when NaCl was partially replaced by sucrose. With the exception of the Cl^- effect on the resting potential, sucrose and choline chloride acted quite similarly on the spike response, altering only V_1 and I_t in proportion to their replacement of Na^+ (see Table I). Although I_t data are not plotted, these are *linear* with (Na^+) within a 10 per cent error ascribed to the graphical analysis.

Note that the shifts in this experiment for V_1 which now may be identified as the sodium potential, reflect an initial gain of intracellular Na^+ during the progress of the experiment. It was predicted from application of the Nernst equation that $(Na^+)_i$ was ~14 mM just after the muscle was dissected and placed in normal Ringer's

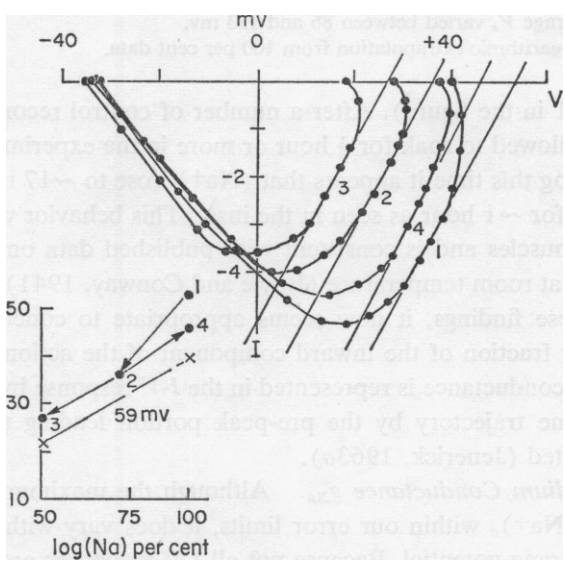

FIGURE 5 The inward current–membrane voltage relationship as affected by Ringer's fluid with varied Na^+ concentration; Nos. 1 and 4 in 110 mM NaCl, No. 2 in 82.5 mM NaCl, No. 3 in 55 mM NaCl. Note in this series that V^* is unchanged as is the peak conductance g_1, indicated by the light lines. The inset plots the equilibrium potentials V_1, in millivolts and a 59 mv/decade line (x———x) against the log of the Na concentration. The shift in V_1 between Responses 1 and 2 is consistent with a slight gain of intrafiber Na^+ during the initial stages of the experiment.

TABLE I*

EXTERNAL SODIUM CONCENTRATION AND V_1

Experiment No.	100 Per cent (110 mM)	75 Per cent (82.5 mM)	50 Per cent (55 mM)	No.
	mv	*mv*	*mv*	
18	47	40	28	31
19	41	35	27	28
20	43	37	28	27
23	—	32	27	12
24	35	27	14	24
25	38	30	20	24
37-1	53	39	27	19
37-2	47	33	25	18
38-1	40	—	25	14
38-2	36	—	21	15
V_1 averages	42.2	35.1	24.2	(212)
V_1 expected‡	42.2	34.8	23.5	

* Data from experiments in which KCl in Ringer's fluid was altered from 1 to 5 mM. The resulting average V_r varied between 74 and 101 mv; the average V_s varied between 86 and 133 mv.

‡ By logarithmic extrapolation from 100 per cent data.

fluid (Response 1 in the figure). After a number of control records were obtained, the muscle was allowed to soak for ½ hour or more in the experimental fluids before proceeding. During this time it appears that $(Na^+)_i$ rose to ~17 mM and was thereafter maintained for ~1 hour as seen in the inset. This behavior was observed in all freshly isolated muscles and is consistent with published data on initial Na^+ gains in Ringer's fluids at room temperature (Boyle and Conway, 1941).

In view of these findings, it now seems appropriate to conclude that Na^+ ion carries the major fraction of the inward component of the action current, and that the peak sodium conductance is represented in the *I-V* response by g_1, and indirectly in the phase plane trajectory by the pre-peak portion leading toward V_1 as was previously suggested (Jenerick, 1963*a*).

Peak Sodium Conductance g_{Na}. Although the maximum g_{Na} in muscle is independent of $(Na^+)_o$ within our error limits, it does vary with the magnitude of the resting membrane potential. Because not all *I-V* responses are as linear in g_1 or (g_{Na}), as those shown in Figs. 1*a* and 5, there is a certain degree of uncertainty in these determinations, as reflected by the vertical scatter in Fig. 6. This presents the relationship between the resting potential V_r and the peak sodium conductance, but because of the difficulty of obtaining the latter data, the figure should be viewed as a tentative one. Fibers which are strongly depolarized by excess KCl or are exposed to low external Na^+ concentrations are liable to give rounded, non-linear responses in

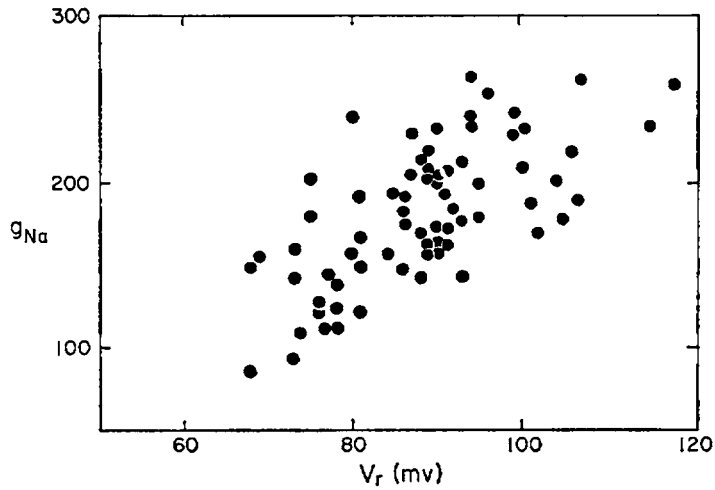

FIGURE 6 The dependence of the peak sodium conductance (in mmhos/cm²) on the resting membrane potential. Each point plots data obtained from a single response.

the g_1 region that are difficult to measure. Because of this uncertainty it cannot be decided whether an S-shaped relation between g_{Na} and V_r is hidden in the figure.

Terminal Membrane Conductance g_2. A striking and consistent feature of the trajectory is a linear portion leading from beyond the second inflection point to the initial value of the negative after-potential. Curvature in the region of k_f if present was always very small and was usually associated with recording problems such as cross-talk from an active adjacent fiber or a mechanical displacement of the electrode by muscular contraction. Since this portion of the trajectory is linear for all practical purposes, its slope k_f may be substituted directly for m in Equation (1.4). An appropriate manipulation of the equations will lead to

$$g_2 = C_m(k_f + k)(k_f/k)$$

Numerous observations have demonstrated that $k > k_f$ and as an approximation, therefore, $g_2 \cong C_m k_f$ which accounts in large measure for the marked linearity of the data in Fig. 7. Incidentally, reference to Fig. 1*b* shows that the g_2 portion of the response is not a minor one and is about 1 msec. in duration.

Normal Action Current Parameters. As mentioned, the purposes of the present study were (*a*) to develop a method by which the action current of a propagated response may be determined, and (*b*) to examine the relationship between various key features of the phase plane trajectory of the propagated response and the major components of the transmembrane action current. Since, the majority of the data are presented to survey and illustrate these relationships, no attempt will be made at this time to examine in detail the separate effects of all the various experimental treatments employed in this study (*i.e.* Ringer's fluid alterations, pH,

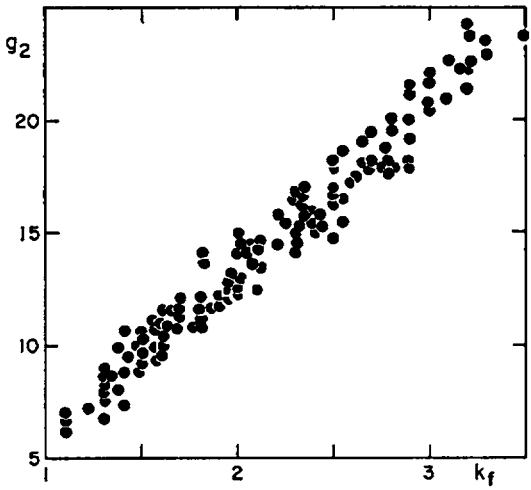

FIGURE 7 The correlation between the rate constant k_f (from Fig. 1*a*) and the terminal membrane conductance g_2 (in mmhos/cm²).

etc.). While the dependence of the phase plane parameters on the magnitudes of the spike and resting potentials was presented recently (Jenerick, 1963*a*) and in past publications from this laboratory, it was not possible until now to determine the significance of these measurements on the response. Because the interrelationship between the action current parameters and the resting or spike potential is not obvious from the preceding sections, Table II was prepared. The data were obtained from that present series of experiments in which KCl concentrations were altered to reset the membrane potential at various levels. The only variable showing a plateau or peak value within the indicated range of resting potentials is g_2. No maxi-

TABLE II

APPROXIMATE VALUES OF ACTION CURRENT VARIABLES*

V_r	V_s	I_i	g_{Na}	I_s	V^*	g_2
mv	*mv*	*ma/cm²*	*mmhos/cm²*	*ma/cm²*	*mv*	*mmhos/cm²*
100-105	140-130	5.8	220	0.85	75	18
90- 95	130-120	4.8	190	0.75	65	21
80- 85	120-110	3.9	160	0.65	55	19
70- 75	110-100	3.1	140	0.5	45	17
65- 70	100- 90	2.4	120	0.4	40	14
60-65	90- 80	1.9	110	0.3	35	11

* These data are taken from the figures and are arranged in order of decreasing resting potential and spike height. All data with the exception of the potentials are directly proportional to membrane capacitance. An assumed value of 5 μf/cm² was used in the preparation of all figures and this table.

mum for I_i or I_o was observed, hence, no evidence for a saturation process (such as a limited amount of "Na carrier") was obtained. Although this finding tends to raise questions about the carrier concept and/or the activation process, it may also be attributed to a variety of incidental reasons (*e.g.* excess carrier in striated muscle membrane).

Calcium Effect on the Action Current. It was previously noted that several parameters of the recorded response are modified by a tenfold increase of Ca ion concentration (Jenerick, 1957). These earlier findings were generally confirmed and extended in the present study which employed the standard Ringer's fluid buffered with histidine to avoid precipitation of Ca (K^+ was varied between 0.5 and 2.5 mM, accounting for the large average V_r). The grand averages of 105 responses from 7 separate experiments are listed in Table III. While these data

TABLE III

CALCIUM EFFECT ON ACTION CURRENT

Parameter	In 1 mM Ca	In 10 mM Ca	Per cent shift
V_r mv	98	97	−1
V_e mv	128	123	−4
V_n mv	20	26	+30
V^* mv	68	74	+9
V_{Na} mv	40	35	−12*
I_i ma/cm²	4.7	2.7	−42
I_o ma/cm²	0.75	0.6	−20
g_{Na} mmhos/cm²	194	196	Negligible
g_2 mmhos/cm²	20.4	19.0	−7

* Attributed to Na gain during initial period of experiment.

were obtained independently from those presented in previous sections, it is of interest to note the close agreement between the entries in Table II, obtained at 2mM Ca, and those in Table III, listed under 1 mM Ca. This illustrates the minor effect of small changes of Ca in this concentration range. The 1 per cent drop in V_r caused by 10 mM Ca was unexpected since a 4 to 6 per cent *increase* was observed in the earlier study. This is attributed to the presence of histidine buffer which of itself increases V_r by several millivolts over its values in a phophate-buffered Ringer's fluid. Other buffers (*e.g.* acetate, ammonium) also affect V_r, and under the circumstances it is tentatively assumed that these changes in V_r by Ca or by buffers reflect some sort of a non-additive salt effect on the membrane or adjacent structures.

Despite a sag in V_{Na} which is ascribed to sodium gain during the experiment, the maximum g_{Na} was unaffected by high Ca fluids as it is in the squid giant axon (Frankenhaeuser and Hodgkin, 1957). Although g_2 was lowered, making it appear that Ca exerts a differential effect on the various membrane conductances, this is

fully accounted for by the decrease in V_s, (*i.e.* the observed shift in g_2 is still consistent with control data listed in Table II).

The most remarkable changes observed in high Ca solutions were the decreases in I_i and I_o, which appeared despite only minor alterations of g_{Na}, V_{Na}, and g_2. Since these measurements refer to events during spike propagation, the results are probably caused by alterations in the *rate* constants of the membrane conductances. Frankenhaeuser and Hodgkin, for example, noted in squid axon that increasing the Ca concentration reduced the rate of rise of the Na^+ conductance following application of a voltage step. By analogy, the postulated slower time course for g_{Na} in muscle (coupled with an increase in V^*), allows less time for I_{Na} to develop before it reaches the maximum permitted by the $g_{Na} - V_{Na}$ relationship. Similar events were reported by them for rates of development of K^+ conductance and may explain the observed decrease of I_o in muscle.

If these suggestions concerning the rate constants of the membrane conductances are valid, it would seem to follow that conduction velocity should be slowed in high Ca fluids. While this was not measured directly, it was observed that k (which is $2\ RC\Theta^2/a$) was lowered by ~50 per cent. It seems likely that R, a, and probably C are not greatly dependent on Ca. If so, it may be inferred that the conduction velocity Θ, was lowered by approximately ~25 per cent, in accordance with the expectation.

The negative after-potential was recently linked with a temporary imbalance which appears during the spike potential between the coulombic charge uptake of the fiber ($q_i = \int I_{in}\, dt$) and the charge loss ($q_o = \int I_{out}\, dt$). Customarily, $q_i > q_o$ and the net accumulation ($q_i - q_o$) apparently serves to charge the membrane capacitance and thus generate V_n (Jenerick, 1963*b*). The Ca ion appears to affect q_i and q_o separately and by so doing alters the magnitude of V_n. For example in Fig. 1*b*, the areas under the curves for inward and outward current correspond to a charge *gain* of 7.4 pmoles/cm^2 ($= 7.1 \times 10^{-7}$ coulombs/cm^2) and a charge *loss* of 5.6 pmoles/cm^2 ($= 5.4 \times 10^{-7}$ coulombs/cm^2). This spike was obtained in a 2 mM Ca^{++} Ringer's fluid. The outward current had greatly subsided by the time the initial portion of the after-potential was reached ($V_n = 18$ mv), and left a net charge accumulation at this time of 1.8 pmoles/cm^2. Presumably, this charge leaks off the membrane capacitance during the after-potential decay. When the Ca concentration was raised to 10 mM, the charge uptake of a comparable fiber was determined to be 7.3 pmoles/cm^2 while the charge loss fell to 5.0 pmoles/cm^2. The *net* accumulation of cationic charge was thus *increased*, as was the negative after-potential which rose to 30 mv. If $\frac{1}{2}$ to 1 pmoles/cm^2 of the net accumulation in these fibers is accounted for by non-specific ion binding, the remaining increase in intrafiber cationic charge concentration is just sufficient to generate the observed negative after-potentials, *viz.*, $V_n = (q_i - q_o)/C$. Similar calculations have been performed on a number of fiber responses and indicate that the main effect of an increased Ca concentration is to

diminish the magnitude of the charge loss, q_o. Since q_i remains relatively unaffected, the net accumulation is thus increased and may account for the observed changes in V_m.

SUMMARY

Certain problems and assumptions in the present method remain untested and unsolved. The more obvious include the applicability of the cable Equation (1.1) to the propagated disturbance and the tacit assumption of a time-independent membrane capacitance during the response. These problems however, are implicit in, or affect, all present approaches to the conduction process, and must remain so until a new model is established.

Within these possible limitations, the present method permits a fairly rapid assessment of the action current under a wide variety of experimental conditions provided these do not alter the capacitance in an unknown fashion. The analysis of the phase plane record may be based on a graphical approach *via* Equation (1.4), or more simply, may employ the empirically derived relations between the recorded phase plane parameters and the membrane properties illustrated in Figs. 2–4, 6, and 7. The net inflow and outflow of charge during the response may also be determined without much increase in computation time. In addition to the required phase plane recording, the response must be obtained simultaneously in V, t coordinates to retrieve the temporal characteristics of the response which are lost in the $\dot{V}$, V plot. Enlarged tracings of such dual records permit a point-by-point plot of the calculated current against voltage or time, as desired.

This paper is publication No. 583 from the Division of Basic Health Sciences, Emory University.

This work was supported by a grant (B-3272) from the National Institute of Neurological Diseases and Blindness.

Received for publication, June 4, 1963.

REFERENCES

BOYLE, P. J., and CONWAY, E. J., 1941, *J. Physiol.*, **100**, 1.
COLE, K. S., 1949, *Arch. Sc. Physiol.*, **3**, 253.
FRANKENHAEUSER, B., and HODGKIN, A. L., 1957, *J. Physiol.*, **137**, 218.
HODGKIN, A. L., and HUXLEY, A. F., 1952, *J. Physiol.*, **117**, 500.
HUBBARD, S. J., 1963, *J. Physiol.*, **165**, 443.
JENERICK, H., 1957, *in* Proceedings of the First National Biophysics Conference, New Haven, Yale University Press, 377.
JENERICK, H., 1959, *J. Gen. Physiol.*, **42**, 923.
JENERICK, H., 1961, *Nature*, **191**, 1074.
JENERICK, H., 1963*a*, *Biophysic. J.*, **3**, 363.
JENERICK, H., 1963*b*, *Nature*, **200**, 1076.
MINORSKY, N., 1947, Introduction to Non-Linear Mechanics, Ann Arbor, J. W. Edwards.
WEIDMANN, S., 1955, *J. Physiol.*, **127**, 213.